ISBN: 978-3-95450-179-3 doi:10.18429/JACoW-FEL2017-TUB04

RECENT ON-LINE TAPER OPTIMIZATION ON LCLS*

Juhao Wu[1†], Kun Fang[1‡], Xiaobiao Huang[1], Guanqun Zhou[1§], Axel Brachmann[1], Claudio Emma[1¶], Chunlei Li[1‖], Eric Li[2], Haoyuan Liu[3], Weihao Liu[4,1], Alberto Lutman[1], Tim Maxwell[1], Claudio Pellegrini[1], Weilun Qin[1**], Tor O. Raubenheimer[1], Alexander Scheinker[5], Cheng-Ying Tsai[1], Bo Yang[6], Chuan Yang[1††], Moohyun Yoon[1‡‡], Brandon W. Zhang[7]
[1]SLAC, Stanford University, Stanford, USA, [2]Palo Alto High School, Palo Alto, USA, [3]Boston University, Boston, MA , USA, [4]NSRL, University of Science and Technology of China, Hefei, Anhui, China, [5]LANL, Los Alamos, USA, [6]Dept. of Mechanical & Aerospace Engineering, University of Texas at Arlington, Arlington, USA [7]Lakeside School, Seattle, USA

Abstract

High-brightness XFELs are in high demand, in particular for certain types of imaging applications. Self-seeding XFELs can respond to a heavily tapered undulator more effectively, therefore seeded tapered FELs are considered a path to high-power FELs in the terawatt level. Due to many effects, including the synchrotron motion, the optimization of the taper profile is intrinsically multi-dimensional and computationally expensive. With an operating XFEL, such as LCLS, the on-line optimization becomes more economical than numerical simulation. Here we report recent on-line taper optimization on LCLS taking full advantage of nonlinear optimizers as well as up-to-date development of artificial intelligence: deep machine learning and neural networks.

TAPERED FEL TO REACH HIGH POWER

Ultra-fast hard X-ray Free electron laser (FEL) pulse providing atomic and femtosecond spatial-temporal resolution [1,2] makes it a revolutionary tool attracting world-wide interests for frontier scientific research. Among these, single particle imaging is one of the applications demanding terawatts (TW) level peak power [3]. To reach TW FEL peak power, using a tapered undulator to keep the FEL further extracting kinetic energy from the high energy electron bunch is an active research direction [4]. However, the FEL after exponential growth saturation has to have good temporal coherence to better respond to a heavily tapered undulator [5]. While the SASE FEL provides high spatial coherence, the temporal coherence is rather poor at exponential growth saturation point. To improve the temporal coherence, seeding approaches: both external [6,7] and self-seeding [8,9] and Slippage-enhanced SASE (SeSASE) [10–13] can produce an FEL pulse with good temporal coherence at the exponential growth saturation region. In this paper, we conduct our study with a self-seeding tapered FEL [14–17].

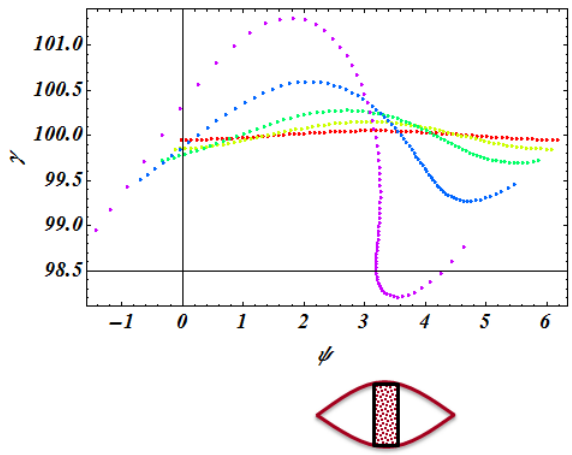

Figure 1: The electrons experience a quarter of a synchrotron motion period and microbunch with a central phase of $\psi \sim \pi$.

The physics changes from high-gain to low-gain FEL after the exponential growth saturates. In the high-gain region, the FEL power grows exponentially [18]:

$$P_{\mathrm{FEL}}(z) = P_0 \exp[z/L_{\mathrm{G}}], \quad (1)$$

where P_0 is the start-up power, L_{G} is the power gain length, and z is the coordinate along the electron forward traveling direction in the undulator. The electrons experience a quarter of a synchrotron motion period from red, yellow, green, blue, and purple; they eventually microbunch with a central coordinate of $\psi \sim \pi$ as shown in Fig. 1. The electrons together with the FEL bucket are illustrated in the lower part of Fig. 1 indicating microbunching at $\psi \sim \pi$.

After the exponential growth saturation, the FEL system evolves into coherence emission. Assuming a transversely round electron beam, a constant bunching factor b_1, and no

* Work supported by the US Department of Energy (DOE) under contract DE-AC02-76SF00515 and the US DOE Office of Science Early Career Research Program grant FWP-2013-SLAC-100164.
† jhwu@SLAC.Stanford.EDU
‡ now at Wells Fargo & Co., San Francisco, CA, USA
§ Ph.D. student from Institute of High Energy Physics, and UCAS, Chinese Academy of Sciences, Beijing, China
¶ Ph.D. student from UCLA, Los Angeles, USA
‖ now at Shanghai Institute of Applied Physics, Chinese Academy of Sciences, Shanghai, China
** Ph.D. student from Peking University, Beijing, China
†† Ph.D. student from NSRL, University of Science and Technology of China, Hefei, Anhui, China
‡‡ on sabbatical leave from Department of Physics, Pohang University of Science and Technology, Pohang, Korea

ISBN: 978-3-95450-179-3 doi:10.18429/JACoW-FEL2017-TUB04

beam loss, so that the peak current I_{pk} is also a constant, the coherent radiation power is [16]:

$$P_{\rm coh} = \frac{Z_0 K^2 \left[JJ\right]^2 I_{pk}^2 b_1^2 z^2}{32\sqrt{2}\pi\sigma_x^2\gamma^2}, \quad (2)$$

where Z_0 is the vacuum impedance, K is the peak undulator parameter, $\sigma_x (= \sigma_y)$ is the rms transverse round electron bunch size, γ is the relativistic factor, and

$$JJ = J_0\left[\frac{K^2}{4\left(1+K^2/2\right)}\right] - J_1\left[\frac{K^2}{4\left(1+K^2/2\right)}\right], \quad (3)$$

with J_0 and J_1 are the zeroth-order and first-order Bessel function.

Due to energy conservation, the resonance energy γ_r evolves according to:

$$\frac{d\gamma_r}{dz} = -\mathcal{A}\frac{K^2 z}{\gamma_r^2}, \quad (4)$$

with

$$\mathcal{A} = \frac{e\left[JJ\right]^2 Z_0 I_{pk} b_1}{2^{11/4} mc^2 \pi w_0 \sigma_x} \sin\left(\psi_r\right), \quad (5)$$

ψ_r is the synchronous phase of the electrons, e is the electron charge, m electron static mass, and w_0 the waist size of the FEL beam.

To maintain the resonance condition for a z-dependent energy, the taper profile is then z-dependent as [16]

$$K(z) \approx K_0\left[1 - \frac{\mathcal{A}\mathcal{B}^2\gamma_{r0}}{2K_0^2}\left(z-z_0\right)^2\right] \text{for } z > z_0, \quad (6)$$

where $\gamma_{r0}^2 = \gamma_r\left(z_0\right)^2$, $K_0 = K(z_0)$, and

$$\mathcal{B} = \frac{4\lambda_r}{\lambda_w}. \quad (7)$$

At this point, we want to make some comments. According to Eq. (4) with Eq. (5), the overall energy exchange between the electrons and the FEL bucket will be almost zero, if we set $\psi_r \sim \pi$. Unfortunately, when the electrons microbunched during the high-gain region, they are microbunched around $\psi \sim \pi$. Indeed, when we do FEL simulation with Genesis code [19], we do find that the electron evolves to a different central phase away from $\psi_r \sim \pi$ when the electrons initially microbunched at the end of the exponential growth region. The details of a particular example are shown in Fig. 2 where the red, green, blue, magenta, cyan, and brown dots stand for the electrons 30, 60, 80, 100, 110, and 120 m into the tapered undulator.

Besides the common feature that the central phase is away from $\psi \sim \pi$, the electrons' central phase is evolving as well as shown schematically as the electron together with the FEL bucket in the right column in Fig. 2. At $z = 120$ m in this particular case, the electron (shown as brown dots) detrapped from the FEL bucket and the FEL reaches the taper

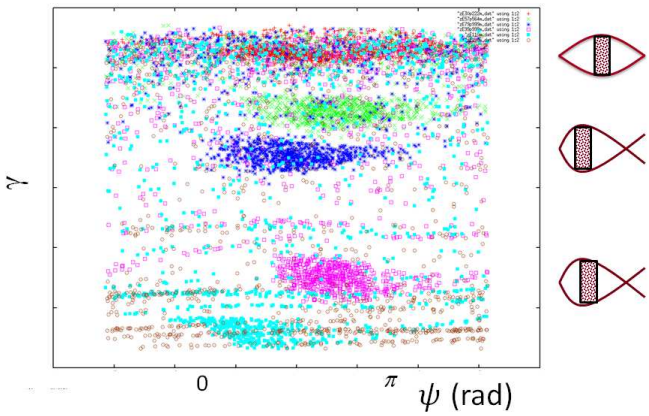

Figure 2: The electrons evolve to a different central phase away from $\psi \sim \pi$ during the post-saturation tapered region.

saturation point, the so-called the second saturation point, to be distinguished from the exponential growth saturation point, the first saturation point.

During the transition region from high-gain (before first saturation) to low-gain in the tapered undulator, the microbunched electrons will have to migrate from $\psi_r \sim \pi$ away to a new phase to achieve best efficiency. In addition, according to Fig. 2, the electron will be doing 2-D motion even in a tapered undulator.

TAPER OPTIMIZATION

For the original LCLS configuration, there were 33 planar undulator sections. Right now, the 9$^{\rm th}$ and the 16$^{\rm th}$ undulator section were removed and replaced with a by-pass chicane together with a grating-based monochromator in section 9 for Soft X-Ray Self-Seeding (SXRSS) and a by-pass chicane with a thin diamond crystal monochromator for Hard X-Ray Self-Seeding (HXRSS) in section 16. Also, the 33$^{\rm th}$ planar undulator is now replaced with a helical undulator. So, the layout is shown in Fig. 3 with each yellow bar standing for one undulator section, the two gaps for two self-seeding station, and the last long yellow bar for the helical undulator.

Taper Profile

Continuous Taper Based on the analysis in the previous section, the taper should be approximately quadratic [16]. In the on-line optimization, we add the quartic term based on the simulation results analyzed in Ref. [16] to have:

$$K(z) = K_0\left[1 - b_2\left(\frac{z-z_2}{L_w - z_2}\right)^2 - b_4\left(\frac{z-z_4}{L_w - z_4}\right)^4\right], \quad (8)$$

where L_w is the undulator length, b_2 and b_4 stand for the strength of the taper ratio; while z_2 and z_4 for the starting point of the quadratic and quartic taper.

Discrete Taper In this case, we optimize piecewise for the 17$^{\rm th}$ to the 32$^{\rm nd}$ undulator sections.

ISBN: 978-3-95450-179-3 doi:10.18429/JACoW-FEL2017-TUB04

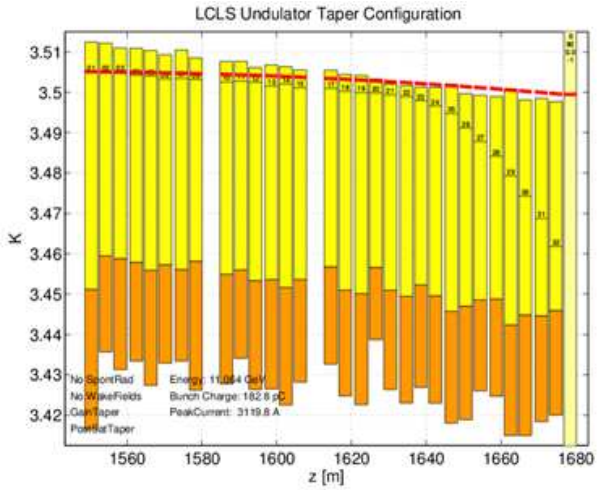

Figure 3: The schematics of the LCLS undulator system. Each yellow bar stands for an undulator section. The two gaps at the 9th and 16th slot host the two monochormators for self-seeding operation.

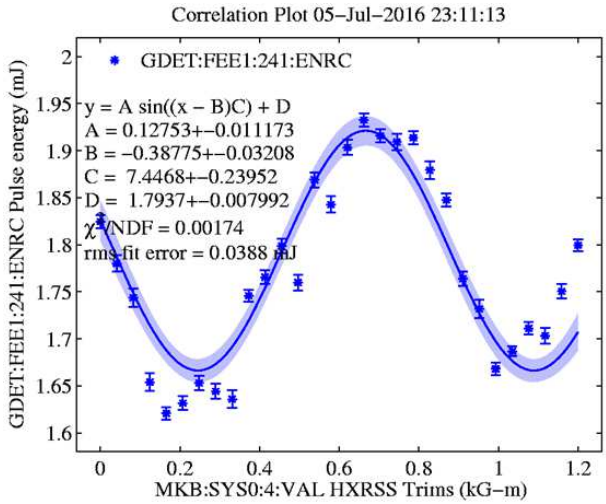

Figure 4: Temporal (phase) matching between the seed and the electron bunching by adjusting the chicane magnet trim coils.

Optimizer

For the past few years, our team has been working on the following algorithms: Robust Conjugate Direction Search (RCDS) [20], Mutil-Object Genetic Algorithm (MOGA) [16], Particle Swarm Optimization (PSO) [21], Extreme Seeking (ES) [22], Simulated Annealing (SA) [23], Reinforcement Learning (RL), and Markov Chain Monte Carlo (MCMC).

Experiment Details in Setting Up the Undulators

In the experiments, we separate the undulator system into three sessions.

Session I Session I consists of sections 1 to 8 for SASE mode, or sections 4 to 8 for 4.5-keV self-seeding mode. The reason why we do not use the first three sections 1 to 3 for the 4.5-keV self-seeding mode is because in the self-seeding mode, the same electron bunch which generates the SASE FEL before the monochromator will be used to amplify the coherent seed in the undulator sections after the monochromator. So, we do not want the slice energy spread of the electron bunch gets too large. In the SASE FEL sections before the monochromator, the electron bunch must not lase too much and maintains a relatively small slice energy spread for later amplification purpose. For a 4.5-keV FEL, the undulator is set up as:

$$K_j = K_{1(,4)}\left[1 - b_1\frac{j-1(,4)}{8-1(,4)}\right] \tag{9}$$

where $j \in [1, 8]$ in SASE mode or $j \in [4, 8]$ for self-seeding.

Session II Session II consists of undulator sections 10 to 15. For $j \in [10, 15]$, the undulator setup is:

$$K_j = (K_8 + \Delta K_{10})\left[1 - b_1\frac{j-10}{5}\right]. \tag{10}$$

Session III Session II consists of undulator sections 17 to 32. For $j \in [17, 32]$, the undulator setup is:

$$\begin{aligned} K_j &= (K_{15} + \Delta K_{17})\left[1 - b_1\frac{j-17}{15}\right. \\ &- \left. b_2\left(\frac{j-j_2}{32-j_2}\right)^2 - b_4\left(\frac{j-j_4}{32-j_4}\right)^4\right]. \end{aligned} \tag{11}$$

In the above setup for the undulator strength, b_1 takes care of the spontaneous emission and the wakefield effect. This is a linear taper. We introduce ΔK_{10} and ΔK_{17} for detuning and phase matching. j_2 and j_4 stand for the starting point for the quadratic and quartic taper.

Additional Experiment Details

Besides the details of setting up the undulator system as mentioned above, some additional details have to be carefully taken care of.

Seeding Phase Matching Even though, in principle, the SASE microbunching should be washed out to have a temporally uniform distribution when the electron bunch traverses the by-pass chicane; there is still an overall temporal (phase) matching to be performed as shown in Fig. 4 using the chicane magnet trim coils.

Orbit and Beta-Matching The by-pass chicane is relative weakly; yet, the orbit of the electrons after traversing the chicane has to be carefully adjusted to make sure the electron

ISBN: 978-3-95450-179-3 doi:10.18429/JACoW-FEL2017-TUB04

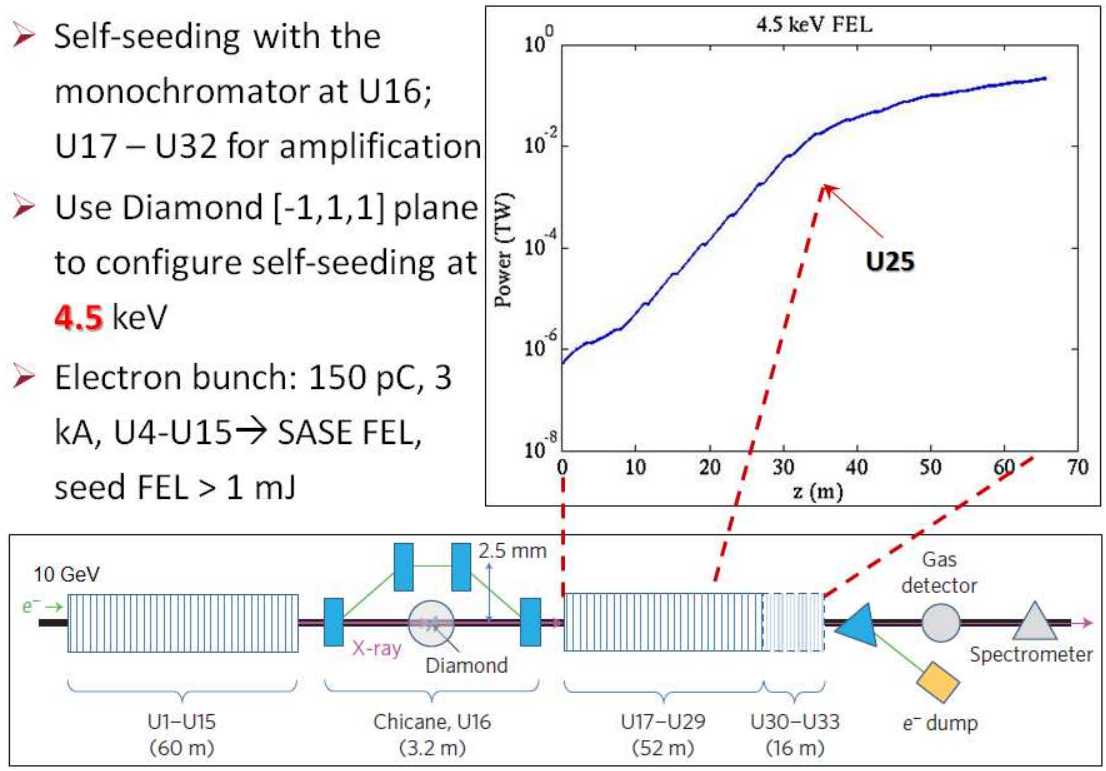

Figure 5: Details of the experiment setup for the 4.5-keV self-seeding tapered FEL.

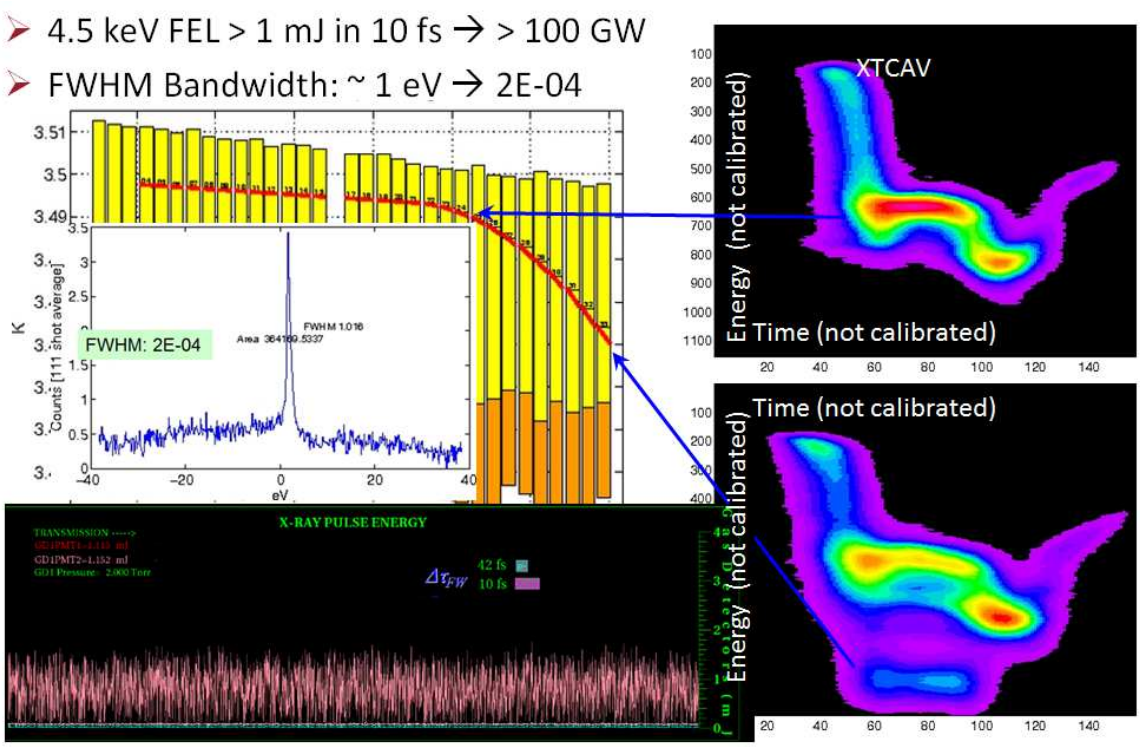

Figure 6: Experimental results from the 4.5-keV self-seeding tapered FEL.

ISBN: 978-3-95450-179-3 doi:10.18429/JACoW-FEL2017-TUB04

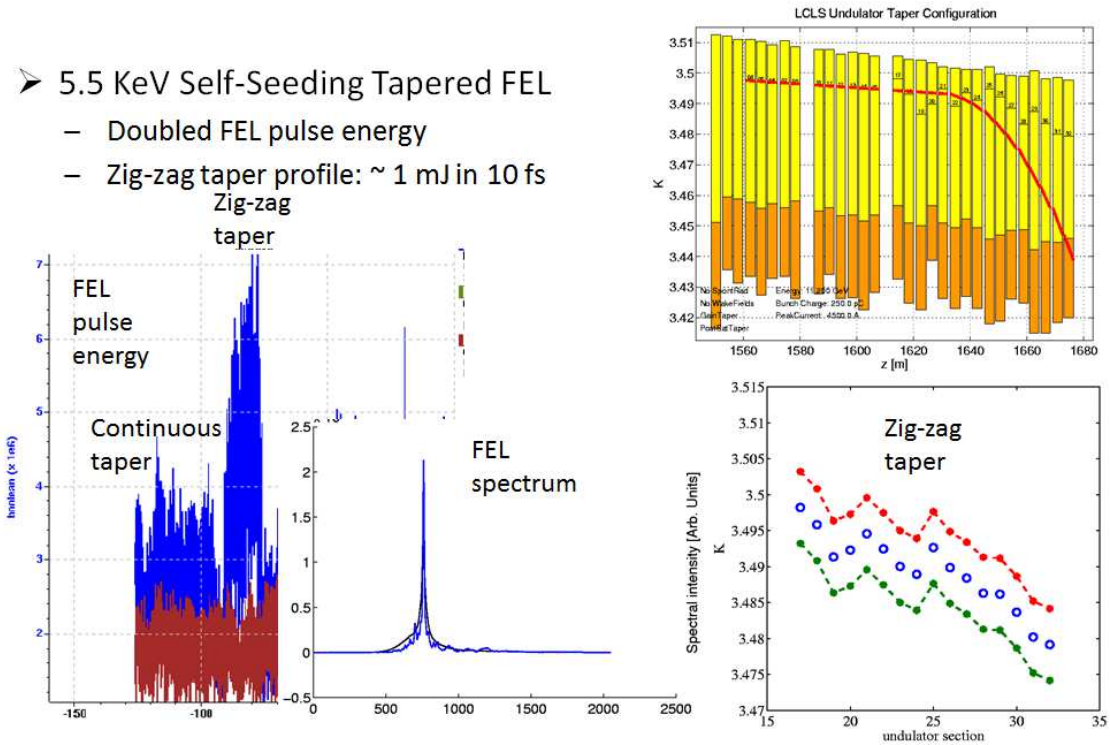

Figure 7: Experimental results from the 5.5-keV self-seeding tapered FEL.

bunch and the seed can spatially best overlap with each other. In addition, rematching the beta-function is important with the by-pass chicane turned on.

Overall Residual Chirp For a self-seeding tapered FEL to have good efficiency, the electron bunch longitudinal phase space should be flat. With an X-band Transverse deflecting cavity (XTCAV), fine tuning of the electron bunch longitudinal phase space is important and necessary.

4.5-keV FEL REACHING 100 GW

With the above mentioned details of theoretical thinking as well as the experimental set up, we here report a 4.5-keV self-seeding experiment generating 100-GW peak power with the LCLS undulator system which provides a maximum of 0.8 % taper ratio, *i.e.*, $[K_0 - K(L_w)]/K_0 \leq 0.8\%$. The details of this experiment setup is shown in Fig. 5. In this experiment, the monochromator is configured with the diamond (-1,1,1) plane as the reflection plane and works in the Bragg condition. The electron bunch has 150-pC charge and a peak current of 3 kA. Undulator sections 1 to 3 were turned off to keep the electron bunch slice energy spread to be relatively small.

The coherent seed at 4.5 keV after the monochromator is about 500 kW in peak power. It is then amplified in the undulator section 17 to 32. The seeded FEL exponential growth saturates at the 25$^{\text{th}}$ undulator. After that the optimum taper is on-line obtained. In this case, a continuous taper model was adopted as shown in Fig. 6. Using the XTCAV, the electron-bunch phase space is clearly shown in the two subplot in the right column in Fig. 6. At the 25$^{\text{th}}$ undulator, the electrons does not lose much energy yet as shown in the upper right subplot. Due to the tapered undulator, the trapped electrons keep losing energy to the FEL, so as shown in the lower right subplot, there is clearly a band of electrons well separated form the others. These electrons in the capture band are the ones who keep giving their kinetic energy to the FEL. This finally leads to an FEL pulse about 10-fs FWHM duration with 1-mJ pulse energy. This indicates that the FEL peak power reaches $P_{\text{FEL}} \sim 100$ GW. The FEL FWHM bandwidth is about 1 eV, or $\Delta\omega/\omega \sim 2 \times 10^{-4}$.

5.5-keV FEL: MACHINE LEARNING

With more and more simulation as well as experimental results, we conducted deep machine learning for the taper optimization. In details, we adopt reinforcement learning for LCLS tapered FEL optimization. Using a Clustering technique, we characterize the XTCAV image as *state* information. Spectrometer and Gas detector measure the FEL pulse energy and give the system *reward*. The undulator K adjustment is then the *action*. With this setup, and a discrete taper setting, the result is a zig-zag taper profile as shown in Fig. 7. In this experiment, we worked with 5.5-keV self-seeding tapered FEL. We started with a continuous taper profile and optimized to get the optimal profile shown as the red curve in the upper right subplot. The corresponding FEL

ISBN: 978-3-95450-179-3 doi:10.18429/JACoW-FEL2017-TUB04

pulse energy is shown as the blue dots in the lower left subplot. With the optimal zig-zag taper, the FEL pulse energy is doubled as shown in the lower left subplot of Fig. 7. In this experiment, for a 5.5-keV self-seeding tapered FEL, we also reached - mJ FEL pulse energy in about 10-fs duration.

CONCLUSION

Over the past a few years, we conducted extensive theoretical and numerical studies, and created on-line optimization packages with these optimizers (both local and global) including reinforcement learning. For the 4.5-keV and 5.5-keV self-seeding tapered FEL at LCLS, the FEL pulse energy can reach 1 mJ with 10-fs duration, generating a peak power of $P_{\mathrm{FEL}} \sim 100$ GW.

REFERENCES

[1] P. Emma *et al.*, "First lasing and operation of an Ångstrom-wavelength free-electron laser", *Nature Photonics* **4**, 641-647 (2010).

[2] T. Ishikawa *et al.*, "A compact X-ray free-electron laser emitting in the sub-angstrom region", *Nature Photonics* **6**, 540-544 (2012).

[3] A. Aquila *et al.*, "The Linac Coherent Light Source single-particle imaging road map", *Structural Dynamics* **2**, 041701 (2015).

[4] N. Kroll, P. Morton, and M. Rosenbluth, "Free-electron lasers with variable parameter wigglers", *IEEE Journal of Quantum Electronics* **17**(8), 1436 (1981).

[5] W. Fawley, Z. Huang, K.-J. Kim, and N. Vinokurov, "Tapered undulators for SASE FELs", *Nuclear Instruments and Methods in Physics Research Section A: Accelerators, Spectrometers, Detectors and Associated Equipment* **483**, 537 (2002).

[6] L.-H. Yu *et al.*, "High-gain harmonic-generation free-electron laser", *Science* **289**, 932-934 (2000).

[7] G. Stupakov, "Using the beam-echo effect for generation of short-wavelength radiation", *Phys. Rev. Lett.* **102**, 074801 (2009).

[8] J. Feldhaus *et al.*, "Possible application of X-ray optical elements for reducing the spectral bandwidth of an X-ray SASE FEL", *Opt. Commun.* **140**, 341-352 (1997).

[9] G. Geloni, V., Kocharyan, and E. Saldin, "A novel self-seeding scheme for hard X-ray FELs", *J. Mod. Opt.* **58**, 1391-1403 (2011).

[10] B. McNeil, N. Thompson, and D. Dunning, "Transform-limited X-ray pulse generation from a high-brightness self-amplified spontaneous-emission free-electron laser", *Phys. Rev. Lett.* **110**, 134802 (2013).

[11] J. Wu, A. Marinelli, and C. Pellegrini, "Generation of longitudinally coherent ultra-high power X-ray FEL pulses by phase and amplitude mixing", in *Proceedings of FEL'12*, Nara, Japan, p. 237.

[12] J. Wu *et al.*, "X-Ray spectra and peak power control with iSASE", in *Proceedings of IPAC'13*, Shanghai, China, p. 2068.

[13] D. Xiang, Y. Ding, Z. Huang, and H. Deng, "Purified self-amplified spontaneous emission (pSASE) free-electron lasers with slippage-boosted filtering", *Phys. Rev. ST Accel. Beams* **16**, 010703 (2013).

[14] Y. Jiao *et al.*, "Modeling and multidimensional optimization of a tapered free electron laser", *Phys. Rev. ST Accel. Beams* **15**, 050704 (2012).

[15] C. Emma, K. Fang, J. Wu, and C. Pellegrini, "High-efficiency, multi-terawatt x-ray free-electron lasers", *Phys. Rev. Accel. Beams* **19**, 020705 (2016).

[16] J. Wu *et al.*, "Multi-dimensional optimization of a terawatt seeded tapered free-electron laser with a multi-objective genetic algorithm", *Nuclear Instruments and Methods in Physics Research Section A: Accelerators, Spectrometers, Detectors and Associated Equipment* **846**, 56 (2017).

[17] A. Mak, F. Curbis, and S. Werin, "Phase-jump method for efficiency enhancement in free-electron lasers", *Phys. Rev. Accel. Beams* **20**, 060703 (2017).

[18] A. Bonifacio, C. Pellegrini, and Narcucci, "Collective instabilities and high-gain regime in a free-electron laser", *Opt. Commun.* **50**(6), 373 (1984).

[19] S. Reiche, "Genesis 1.3: a fully 3d time-dependent FEL simulation code", *Nuclear Instruments and Methods in Physics Research Section A: Accelerators, Spectrometers, Detectors and Associated Equipment*, **429**(1), 243-248 (1999).

[20] X. Huang, J. Corbett, J. Safranek, and J. Wu, "An algorithm for online optimization of accelerators", *Nuclear Instruments and Methods in Physics Research Section A: Accelerators, Spectrometers, Detectors and Associated Equipment* **726**, 77-83 (2013).

[21] K. Fang, C. Pellegrini, J. Wu, S. Hsu, and C. Emma, "Recent study in iSASE", in *Proceedings of FEL'15*, Daejeon, Korea, p. 393.

[22] A. Scheinker, X. Huang, and J. Wu, "Minimization of betatron oscillations of electron beam injected into a time-varying lattice via extremum seeking", *IEEE Transactions on Control Systems Technology* 2017, DOI. 10.1109/TCST.2017.2664728.

[23] L. Gupta, K. Fang, and J. Wu, "Optimization of an improved SASE (iSASE) FEL", pp. 1881, in *Proceedings of IPAC'15*, Richmond, VA, USA.